Article

Development of Robust CuNi Bimetallic Catalysts for Selective Hydrogenation of Furfural to Furfuryl Alcohol under Mild Conditions

Deqin He [1,†], Zheng Liang [2,†], Juwen Gu [1], Xuechun Sang [1], Yujia Liu [1,3,4,*] and Songbai Qiu [1,3,4,*]

[1] School of Chemical Engineering and Light Industry, Guangdong University of Technology, Guangzhou 510006, China
[2] Guangzhou Key Laboratory of Clean Transportation Energy and Chemistry, Guangzhou 510006, China
[3] Guangzhou Institute of Energy Conversion, Chinese Academy of Sciences, Guangzhou 510640, China
[4] Guangdong Provincial Key Laboratory of Plant Resources Biorefinery, Guangzhou 510006, China
* Correspondence: yujia.liu@gdut.edu.cn (Y.L.); qiusb@gdut.edu.cn (S.Q.)
† These authors contributed equally to this work.

Abstract: Furfuryl alcohol represents a pivotal intermediate in the high-value utilization of renewable furfural, derived from agricultural residues. The industrial-scale hydrogenation of furfural to furfuryl alcohol typically employs Cu-based catalysts, but their limited catalytic activity necessitates high-temperature and high-pressure conditions. Here, we develop robust CuNi bimetallic catalysts through direct calcination of dried sol–gel precursors under H_2 atmosphere, enabling the complete conversion of furfural to furfuryl alcohol under mild conditions. By adjusting the calcination atmosphere and introducing small amounts of Ni, we achieve the formation of highly dispersed, ultrasmall Cu nanoparticles, resulting in a significant enhancement of the catalytic activity. The optimized 0.5%Ni-10%Cu/SiO_2-CA(H_2) catalyst demonstrates superior catalytic performance, achieving 99.4% of furfural conversion and 99.9% of furfuryl alcohol selectivity, respectively, at 55 °C under 2 MPa H_2, outperforming previously reported Cu-based catalysts. The excellent performance of CuNi bimetallic catalysts can be attributed to the highly dispersed Cu nanoparticles and the synergistic effect between Cu and Ni for H_2 activation. This research contributes to the rational design of Cu-based catalysts for the selective hydrogenation of furfural.

Keywords: furfural; selective hydrogenation; CuNi bimetallic catalyst; furfuryl alcohol

1. Introduction

In light of the growing consensus on the urgent need to address dramatic climate change, there is a broad international agreement on the necessity of carbon peaking and carbon neutrality. As opposed to fossil resources, the sustainable development of biomass-derived chemicals and fuels is considered a crucial step towards achieving carbon neutrality in the future [1–4]. Among the known biomass-derived platform molecules, furfural is the only renewable basic organic chemical currently available on a large scale from sugar-containing biomass feedstocks; thus, it facilitates the transition to the biorefinery industry in the production of high-value chemicals [5–8]. The catalytic hydrogenation of furfural to furfuryl alcohol represents a pivotal step in the furfural transformations, as more than 60% of furfural is industrially used to produce furfuryl alcohol, which is then broadly applied in downstream manufacturing resins, adhesives, synthetic fibers, etc. [9–11].

The industrial-scale hydrogenation of furfural to furfuryl alcohol typically employs Cr-promoted Cu-based catalysts, but their limited catalytic activity necessitates operation at high temperature (180 °C) and high H_2 pressure (7–10 MPa) [10,12]. Nevertheless, the severe reaction conditions inevitably result in additional side reactions, leading to the formation of excessive undesired products, such as tetrahydrofurfuryl alcohol, methyl

furan, and furan. Therefore, the rational design and preparation of highly active Cu-based catalysts for furfural hydrogenation under mild conditions still presents a significant challenge [13]. In recent years, many attempts have been made to effectively improve the catalytic performance by applying bimetallic catalysts containing Pt, Pd, Ir, Ni, Co, and Cu [10,14,15]. For instance, bimetallic PtCo/C catalysts have been observed to achieve 100% conversion of furfural to furfuryl alcohol at 35 °C and 0.1 MPa in water. The application of CoMoB alloy, Na-Cu@TS-1, and CuCo@/Zn@NPC-600 catalysts has also been reported to achieve high furfuryl alcohol yield (>90%) at 100–140 °C and 1–2 MPa H_2 [16,17]. Hence, it is highly desirable to develop non-noble metal-based catalysts capable of achieving complete and selective conversion under mild conditions (preferably < 100 °C). In comparison to Cu, Ni displays a greater propensity to react with both the furan ring (C=C) and the carbonyl group (C=O) of furfural molecule [18,19]. This is attributable to the stronger interaction between Ni and the π-bonds of the furan ring. To further enhance the activity and selectivity of furfural hydrogenation, the preparation of CuNi bimetallic catalysts with the achievement of high metal dispersion is an alternative route to facilitate the generation of a greater number of active sites [20,21].

This study presents a rational design strategy for the preparation of robust Cu-based catalysts for the selective hydrogenation of furfural. The synthesis of high-performance CuNi bimetallic catalysts is successfully achieved through a modified sol–gel method, wherein citric acid (CA) acts as a complexing agent, facilitating the uniform dispersion of metal precursors within the silica gel network during sol–gel formation and drying. The following calcination under H_2 atmosphere transforms CA into protective carbon species that surround the metal nanoparticles, thereby inhibiting their migration and agglomeration. Subsequently, excess residual carbon species on the metal surface are removed by H_2 reduction, resulting in highly dispersed $CuNi/SiO_2$ catalysts with small particle sizes of 2.2 nm, appropriate ratios of Cu^+/Cu^0, and enhanced H_2 activation via Ni. The bimetallic CuNi catalysts demonstrate excellent catalytic performance in the selective hydrogenation of furfural. The most effective catalyst, 0.5%Ni-10%Cu/SiO$_2$-CA(H$_2$) (CA: citric acid addition; H_2: H_2 atmosphere calcination), achieves a furfural conversion of 99.4% and a furfuryl alcohol selectivity of 99.9% at 55 °C and 2 MPa H_2.

2. Results and Discussion

2.1. Catalyst Synthesis and Characterization

The synthesis method of ultrasmall CuNi nanoparticles on SiO_2 is illustrated in Figure 1, which is discussed briefly using the synthesis of 0.5%Ni-10%Cu/SiO$_2$-CA as a representative example. The initial step involves the transformation of a mixed solution comprising $Cu(NO_3)_2 \cdot 3H_2O$, $Ni(NO_3)_2 \cdot 6H_2O$, citric acid (CA), and ethyl orthosilicate (TEOS) into a uniform gel through a series of coordination and hydrolysis reactions. The subsequent calcination of the dried gel under H_2 atmosphere yields the 0.5%Ni-10%Cu/SiO$_2$-CA(H$_2$) catalyst, comprising ultrasmall CuNi nanoparticles.
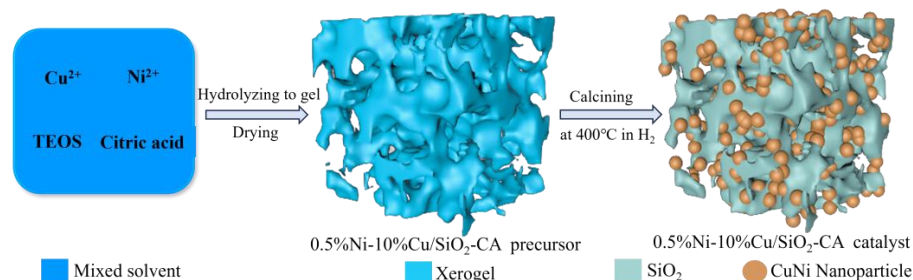

Figure 1. Schematic illustration for the synthesis of 0.5%Ni-10%Cu/SiO$_2$-CA.

In contrast to traditional heat treatment methods, which involve calcination of catalyst samples in N_2 (air) followed by H_2 reduction, the direct calcination of precursors under H_2 atmosphere offers several advantages in the production of ultrafine metal nanoparticles.

The X-ray diffraction (XRD) patterns of 10%Cu/SiO$_2$-CA catalysts prepared using different heat treatment methods are shown in Figure 2a. The diffraction peaks at 43.4°, 50.6°, and 74.3° are attributed to the (111), (200), and (220) planes of metallic Cu [22], respectively. The diffraction peaks at 36.5°, 42.4°, 61.5°, and 73.7° correspond to the (111), (200), (220) and (311) planes of Cu$_2$O [23], respectively. In comparison to the 10%Cu/SiO$_2$-CA(N$_2$-H$_2$) and 10%Cu/SiO$_2$-CA(N$_2$-Air-H$_2$) catalysts prepared via multi-step treatments, the 10%Cu/SiO$_2$-CA(H$_2$) catalyst exhibits a reduced and more diffuse diffraction intensity of Cu and Cu$_2$O, indicating that direct calcination under H$_2$ atmosphere plays a crucial role in promoting the formation of the ultrasmall nanoparticle size and high dispersion of the active phase. Notably, the addition of Ni in an optimal amount has been observed to further enhance the dispersion of the active phase. The addition of 0.5% Ni during the preparation process results in a significant decrease in the intensity of the diffraction peaks (Figure 2b). However, when the Ni content exceeds 0.5%, the diffraction peaks become increasingly intense and sharp, accompanied by a shift to higher angles (Figure S1). This phenomenon can be attributed to the larger atomic radius of Cu in comparison to that of Ni. The doping of Ni into Cu leads to a contraction of the lattice unit, resulting in the shift of the diffraction peaks to a higher angle [24,25]. This indicates that adding a small amount of Ni to Cu leads to a reduction in the lattice size, which is conducive to the dispersion of nanoparticles. However, as the Ni content is further increased, the formation of the CuNi alloy phase hinders the dispersion of the active phase.
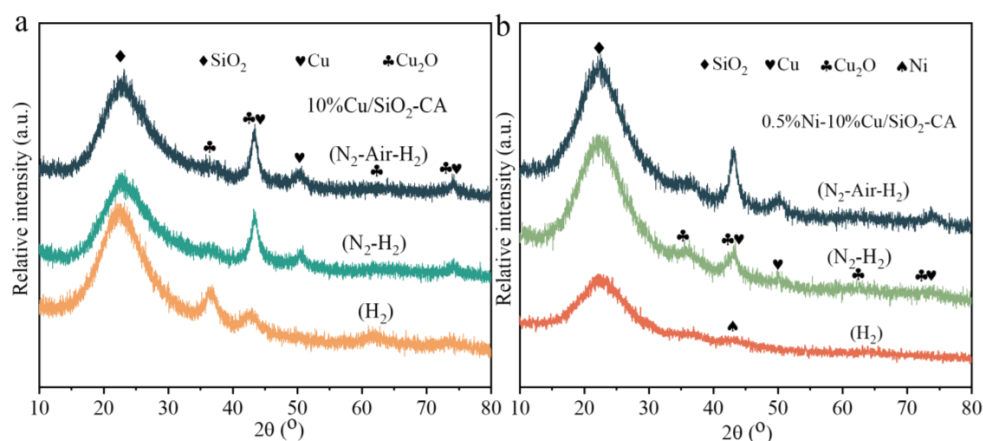

Figure 2. XRD patterns of (**a**) 10%Cu/SiO$_2$-CA and (**b**) 0.5%Ni-10%Cu/SiO$_2$-CA calcined in different atmospheres.

The structures of the typical 0.5%Ni-10%Cu/SiO$_2$-CA(H$_2$) and 10%Cu/SiO$_2$-CA (H$_2$) catalysts were then further characterized. Both catalysts exhibit comparable specific surface areas (about 630.0 m^2·g^{-1}) and pore size distributions of about 3.0 nm (Figure S3 and Table S1). Moreover, scanning electron microscopy (SEM) images show that both catalysts are constituted of spherical SiO$_2$ loaded with ultrafine metal nanoparticles (Figure S2), indicating a similar structure between the 0.5%Ni-10%Cu/SiO$_2$-CA(H$_2$) and 10%Cu/SiO$_2$-CA(H$_2$) catalysts. The detailed structure of the 0.5%Ni-10%Cu/SiO$_2$-CA(H$_2$) catalyst was further characterized by transmission electron microscopy (TEM). As illustrated in Figure 3a, the uniform nanoparticles with an average diameter of 2.2 nm exhibit excellent dispersion on the SiO$_2$ surface. The lattice fringe of 0.205 nm is attributed to the (111) plane of Cu (Figure 3b), which is smaller than that of the conventional Cu (111) plane (0.21 nm) [26]. This suggests that the lattice has undergone contraction due to the addition of Ni, as confirmed by the XRD observations [27]. Elemental mapping through energy-dispersive X-ray spectrometry (EDS) reveals that Ni and Cu species are distributed uniformly throughout the 0.5%Ni-10%Cu/SiO$_2$-CA(H$_2$) catalyst (Figure 3c–e), indicating that the doped Ni is also distributed uniformly along with the Cu nanoparticles. X-ray photoelectron spectroscopy (XPS) was then employed to investigate the elemental compositions and chemical states of

the typical catalysts. The XPS survey spectra indicate that both catalysts contain Cu, Si, and O (Figure 4a). In the Ni $2p$ spectra (Figure 4b) of the 0.5%Ni-10%Cu/SiO$_2$-CA (H$_2$) catalyst, the primary peaks are attributed to Ni^0 and Ni^{2+} in Ni $2p_{1/2}$ and Ni $2p_{3/2}$, respectively. The Ni^0 peaks are observed at 852.6 and 870.2 eV, while the Ni^{2+} peaks are observed at 856.3 and 874.1 eV, respectively [28]. In addition, the Cu $2p$ XPS spectra (Figure 4c) are similar between the 0.5%Ni-10%Cu/SiO$_2$-CA(H$_2$) and 10%Cu/SiO$_2$-CA(H$_2$) catalysts. The Cu $2p$ spectra are the only detected Cu^0/Cu$^+$ species (932.7 eV for Cu $2p_{3/2}$ and 934.5 eV for Cu $2p_{1/2}$) [29,30]. As shown in Figure 4d, the Cu-LMM Auger spectra reveal the existence of Cu^0 and Cu$^+$. As shown in Table S4, the Cu^0/Cu$^+$ ratio is lower on the 0.5%Ni-10%Cu/SiO$_2$-CA(H$_2$) catalyst compared to the 10%Cu/SiO$_2$-CA(H$_2$) catalyst, indicating that Ni doping hinders the reduction of Cu species to Cu^0, which could influence the catalytic performance.

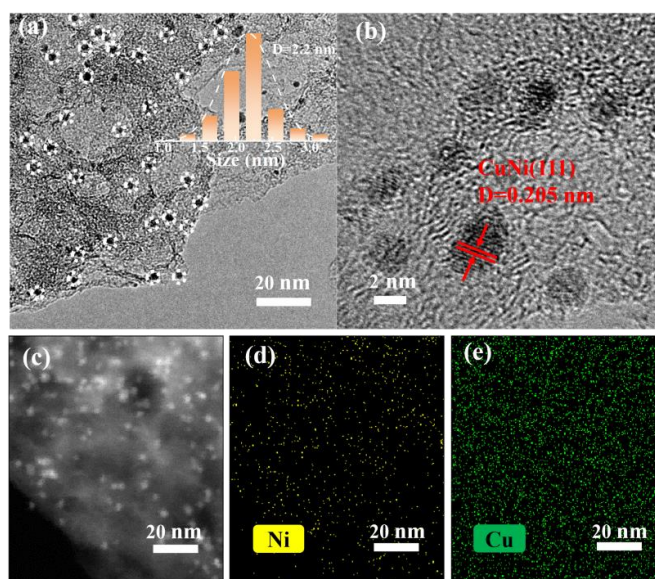**Figure 3.** HAADF-STEM images (**a**,**b**) and element mapping images (**c**–**e**) of 0.5%Ni-10%Cu/SiO$_2$-CA(H$_2$) catalyst.
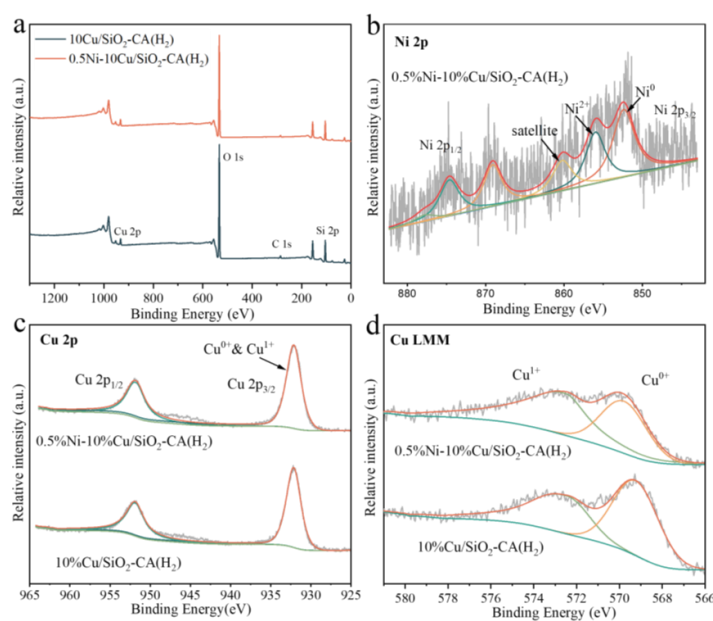

Figure 4. In situ XPS spectra of typical samples: (**a**) full—scan; (**b**) Ni 2p; (**c**) Cu 2p; (**d**) Cu LMM AES.

2.2. Hydrogenation Performance

Furthermore, the catalytic performance of CuNi bimetallic catalysts was assessed in the furfural hydrogenation. We first evaluated the performance of 10%Cu/SiO$_2$-CA catalysts prepared by different heat treatment methods at 55 °C and 4 MPa H$_2$. As shown in Figure 5a, both the 10%Cu/SiO$_2$-CA catalysts exhibit exceptional selectivity towards furfuryl alcohol, reaching over 99.0%. Notably, the catalytic efficiency of the 10%Cu/SiO$_2$-CA catalyst prepared by direct calcination under H$_2$ atmosphere is significantly higher than that of the catalysts prepared by traditional heat treatment methods. The 10%Cu/SiO$_2$-CA(H$_2$) catalyst demonstrates nearly complete conversion of furfural, whereas the furfural conversion for the 10%Cu/SiO$_2$-CA(N$_2$-H$_2$) and 10%Cu/SiO$_2$-CA(N$_2$-Air-H$_2$) catalysts is only 35.0% and 48.9%, respectively. This is further supported by the XRD results (Figure 2a), which show that direct calcination under H$_2$ atmosphere improves the dispersibility of the active phase within the catalyst, leading to enhanced furfural conversion. Then, we performed the test by varying the calcination temperature to identify the optimal catalysts. As shown in Figure S4, the rate of furfural conversion demonstrates a gradual increase with the rising calcination temperature.
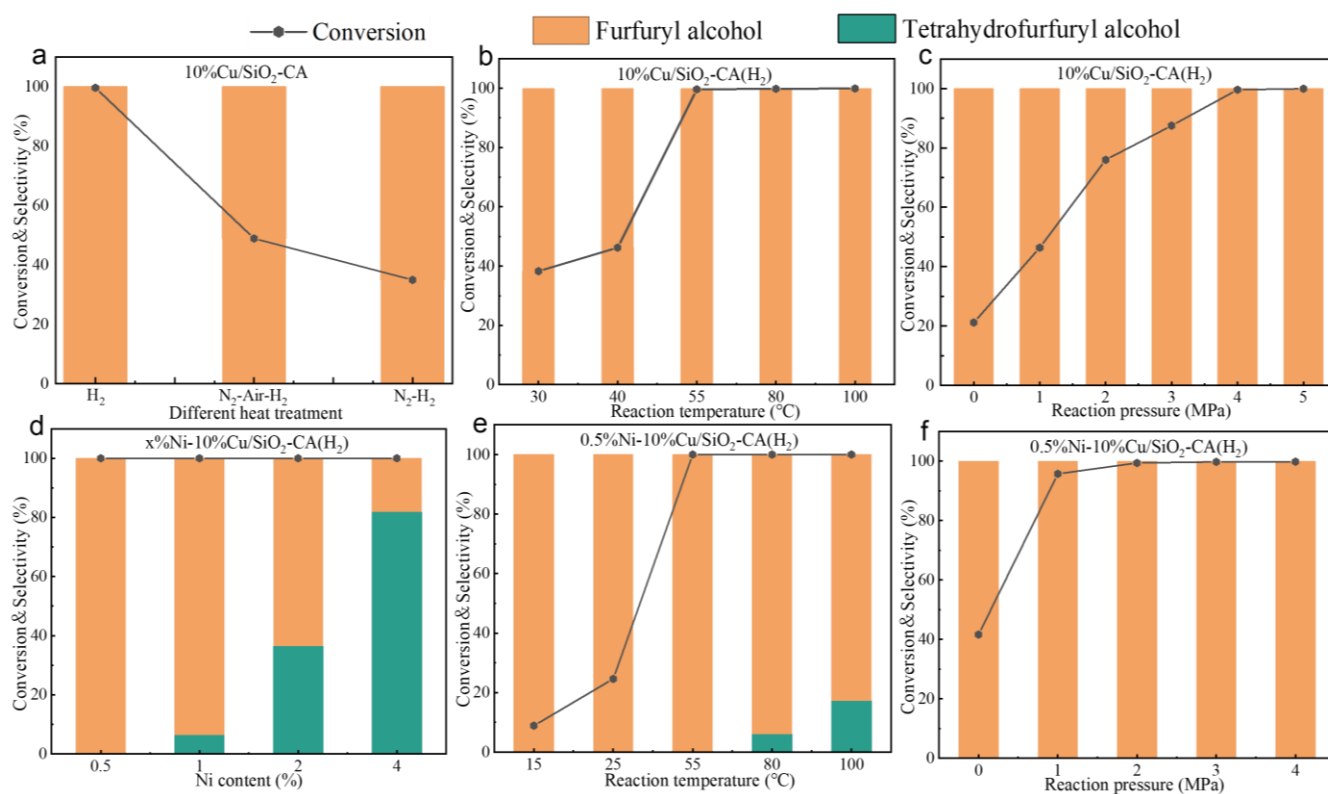

Figure 5. Catalytic performance of 10%Cu/SiO$_2$-CA with different influencing factors: (**a**) different heat treatments (55 °C, 4 MPa H$_2$), (**b**) different reaction temperatures (4 MPa H$_2$), and (**c**) different reaction pressures (55 °C). Catalytic performance of x%Ni-10%Cu/SiO$_2$-CA(H$_2$) with different influencing factors: (**d**) different Ni contents (55 °C, 4 MPa H$_2$), (**e**) different reaction temperatures (4 MPa H$_2$), and (**f**) different reaction pressures (55 °C). Reaction conditions: 0.32 g furfural, 2.88 g isopropanol, 0.089 g catalyst, 2 h.

At a reduction temperature of 300 °C, the catalyst reduction is incomplete, resulting in incomplete exposure of active sites. This leads to a furfural conversion of only 91.5%. Increasing the reduction temperature to 400 °C, leads to a furfural conversion of 99.7%, indicating complete catalyst reduction. Next, we investigated the influence of reaction conditions on the 10%Cu/SiO$_2$-CA(H$_2$) catalyst prepared via direct calcination under H$_2$ atmosphere at 400 °C. As shown in Figure 5b, the furfural conversion increases

with the increasing reaction temperature, reaching complete conversion at 55 °C. The furfural conversion also shows a monotonically increasing trend with the increasing reaction pressure, ultimately reaching 99.6% at 4 MPa (Figure 5c). Throughout the optimization of the preparation and reaction conditions, the selectivity towards furfural alcohol over the 10%Cu/SiO$_2$-CA(H$_2$) remains at 100%. Furthermore, the Cu-based catalyst is demonstrated to have significant advantages in achieving the directional conversion of furfural to furfural alcohol.

Subsequently, we further explored the promotional effect of Ni doping. We systematically screened a series of x%Ni-10%Cu/SiO$_2$-CA(H$_2$) catalysts with varying Ni contents at 55 °C. As shown in Figure 5d, all the catalysts show excellent hydrogenation performance, with the complete conversion of furfural within 2 h. However, the Ni contents above 1.0% lead to the formation of unavoidable saturated hydrogenation products. Increasing the Ni content enhances the selectivity for tetrahydrofurfuryl alcohol. These results suggest that the Ni content in the x%Ni-10%Cu/SiO$_2$ -CA(H$_2$) catalysts is a crucial factor in achieving high selectivity and activity towards furfuryl alcohol. We found that the optimal Ni content was 0.5%. Similarly, in our search for the optimal reaction temperature, as shown in Figure 5e, the furfural conversion can reach nearly 100% at 55 °C. Further increasing the reaction temperature results in the formation of tetrahydrofurfuryl alcohol. Notably, the 0.5%Ni-10%Cu/SiO$_2$-CA(H$_2$) catalyst exhibits higher hydrogenation activity than the 10%Cu/SiO$_2$-CA(H$_2$) catalyst, even under low pressure, achieving a 99.4% furfural conversion at 2 MPa (Figure 5f). These experimental findings demonstrate that a modest amount of Ni doping (0.5%) markedly enhances the hydrogenation capability of the 10%Cu/SiO$_2$-CA(H$_2$) catalyst, enabling directional conversion of furfural to furfural alcohol under mild conditions (2.0 MPa H$_2$, 55 °C). As evidenced by the data in Table 1, the 0.5%Ni-10%Cu/SiO$_2$-CA(H$_2$) catalyst displays superior furfural hydrogenation performance with remarkable furfuryl alcohol selectivity under mild conditions compared to other reported Cu-based catalysts.

Then, we performed a stability test. As shown in Table S6, the catalyst activity exhibits a slight decline after two cycles and a more pronounced reduction after three cycles, accompanied by a 20% decrease in furfural conversion. XRD analysis (Figure S7) after the reaction reveals that the diffraction peaks at 36.5°, 42.4°, 61.5°, and 73.7° become progressively sharper, indicating the agglomeration of Cu nanoparticles during the reaction, resulting in an increase in the catalyst particle size and a decrease in the catalytic activity.

2.3. Mechanism Investigation

To elucidate the effect of Ni doping on the catalytic performance, we further investigated the key factors influencing its high-efficiency hydrogenation of furfural. Hydrogen temperature-programmed reduction (H$_2$-TPR) was employed to compare the reducibility of the typical 10%Cu/SiO$_2$-CA(H$_2$) and 0.5%Ni-10%Cu/SiO$_2$-CA(H$_2$) catalysts.

As shown in Figure 6a,b, all the samples show a single reduction peak within a low-temperature range (170−180 °C), attributed to the reduction of surface oxide species on the Cu nanoparticles [16,31]. The 0.5%Ni-10%Cu/SiO$_2$-CA(H$_2$) catalyst (179.6 °C) possesses a slightly higher reduction temperature in comparison to the 10%Cu/SiO$_2$-CA(H$_2$) catalyst (173.2 °C), thereby indicating that Ni doping slightly represses the reduction of surface oxide species. This finding is in agreement with the results obtained from Cu-LMM Auger spectra. Then, hydrogen temperature-programmed desorption (H$_2$-TPD) was also performed on typical 10%Cu/SiO$_2$-CA(H$_2$) and 0.5%Ni-10%Cu/SiO$_2$-CA(H$_2$) catalysts to further explore the interaction between hydrogen and the active sites (Figure 6c,d). The 10%Cu/SiO$_2$-CA(H$_2$) catalyst reveals two desorption peaks at 534.0 °C and 728.5 °C, but only one peak at 539.4 °C for the 0.5%Ni-10%Cu/SiO$_2$-CA(H$_2$) catalyst. These results show that Ni doping weakly reduces the adsorption of active hydrogen on the catalyst surface, potentially facilitating furfural hydrogenation [32,33].
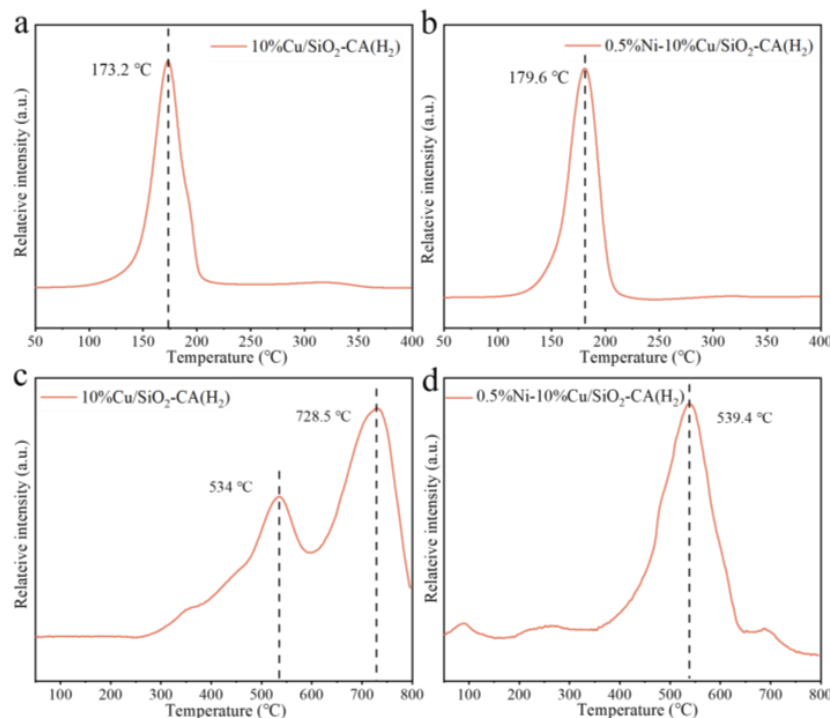
Figure 6. (**a**,**b**) H$_2$-TPR and (**c**,**d**) H$_2$-TPD profiles of typical samples.

Table 1. Performance of 0.5%Ni-10%Cu/SiO$_2$-CA(H$_2$) and comparison with other Cu-based catalysts for selective hydrogenation of furfural.

Catalysts	T/°C	H$_2$/MPa	t/h	Furfural Conversion/%	Furfuryl Alcohol Selectivity/%	Ref.
0.5%Ni-10%Cu/SiO$_2$-CA(H$_2$)	55	1	2	95.7	99.9	This work
0.5%Ni-10%Cu/SiO$_2$-CA(H$_2$)	55	2	2	99.4	99.9	This work
NiCu$_{0.33}$/C	120	1.5	12	96.7	93.8	[34]
Na-Cu@TS-1	110	1	2	93	98.1	[16]
Cu$_2$Ni$_1$AlO$_y$	120	1.6	1.5	98	99	[35]
Cu$_3$Co$_1$/MgAlO$_X$	110	2	2	100	99.9	[33]
CuNiO$_X$(1/1)-150	150	3	0.75	100	97	[30]
Cu/AC−SO$_3$H	105	0.4	2	99.9	99.9	[3]
Pd$_1$Cu$_{216}$	50	0.15	7	40.1	99.9	[36]
Cu/MgO-350	110	2	1.3	99.9	99.9	[29]
CuCo/MgO-0.04	100	2	1	100	99.4	[37]
Cu−Pt@TMS	110	1	1.5	98.4	99.6	[38]
2-Cu/C-400	170	2	3	99.6	99.3	[39]
NiCoCuZnFe/C- 800	120	3	9	100	100	[17]

Table S4 presents Cu-LMM Auger spectra data for the 10%Cu/SiO$_2$-CA and 0.5%Ni-10%Cu/SiO$_2$-CA(H$_2$) catalysts. The 0.5%Ni-10%Cu/SiO$_2$-CA(H$_2$) catalyst exhibits a higher Cu$^+$ percentage (59.63%) than the 10%Cu/SiO$_2$-CA catalyst (38.70%), indicating that Ni doping hinders the catalyst reduction; this is consistent with the H$_2$-TPD results. The furfuryl-TPD profiles (Figure 7) show a slightly higher furfural desorption temperature for 0.5%Ni-10%Cu/SiO$_2$-CA(H$_2$) (256 °C) compared to 10%Cu/SiO$_2$-CA(H$_2$) (242.5 °C), suggesting enhanced furfural adsorption, possibly due to the increased Cu$^+$ content.
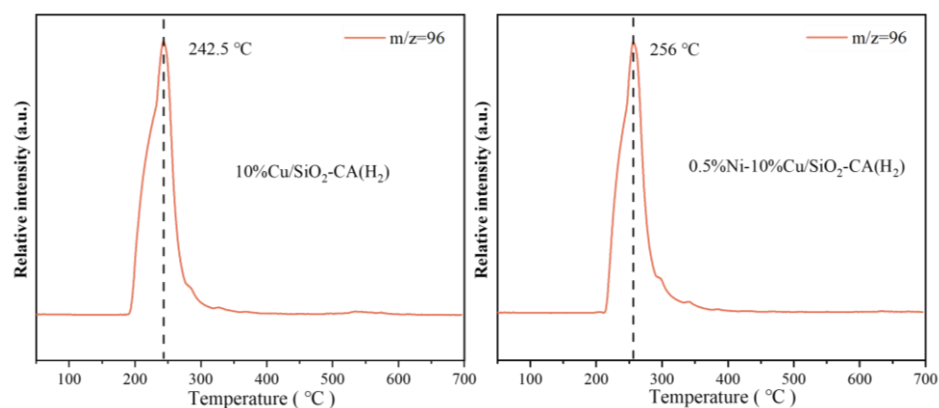
Figure 7. Furfural-TPD/MS profiles over the 10%Cu/SiO₂-CA and 0.5%Ni-10%Cu/SiO₂-CA catalysts.

As previously documented in the literature [30], the DFT calculations indicate that $Cu_2O(111)$ exhibits the most robust H* adsorption and the lowest H_2 dissociation barrier among Cu(111), Cu_3Ni_1 (111), Cu_2Ni_2 (111), Cu_1Ni_3(111), and $Cu_2O(111)$. This observation suggests that Cu^+ sites are the primary H_2 adsorption and dissociation sites in furfural hydrogenation. Furthermore, the DFT calculations also indicate that furfural adsorption on Cu(111) is relatively weak (-0.91 eV), occurring only via the carbonyl oxygen. Adding Ni to form CuNi alloys significantly strengthens adsorption (-1.18 to -1.99 eV), as does $Cu_2O(111)$ (-1.65 eV). Enhanced interaction between the furan ring and CuNi surfaces, indicated by increased bond lengths in adsorbed furfural and shorter surface–adsorbate distances, suggests that both the carbonyl and furan C=C groups are involved in stabilization [40–42]. These results, along with prior characterization data, explain the high performance of the 0.5%Ni-10%Cu/SiO₂-CA(H₂) catalyst in furfural hydrogenation; this is attributable to the enhanced furfural adsorption and H_2 activation by CuNi alloys and Cu^+ species.

Overall, the experimental results demonstrate that doping Ni into Cu nanoparticles leads to lattice contraction and slightly weakens Cu reduction. This prevents the aggregation of Cu nanoparticles during synthesis, improving the dispersion of the active phase. Furthermore, the increased number of Cu^+ sites due to Ni doping promotes furfural adsorption, leading to higher reactant adsorption on the catalyst surface. Finally, enhanced furfural adsorption and H_2 activation, facilitated by Ni doping, results in more efficient furfural hydrogenation and improved catalytic activity.

3. Materials and Methods

3.1. Catalyst Preparation

All reagents were commercially available and used without further purification. Furfural (99%), furfuryl alcohol (98%), isopropanol (99.5%), copper nitrate trihydrate (99%), nickel nitrate hexahydrate (98%), citric acid monohydrate (CA; 99.8%), ethyl orthosilicate (TEOS; 98%), commercial 5% Ru/C, commercial 5% Pt/C, and commercial 5% Pd/C were purchased from Shanghai Aladdin Biochemistry Technology Co., Ltd. (Shanghai, China). Gases (99.999% H₂, 10% H₂/He, and 99.999% N₂) were obtained from Guangzhou Yuejia Gas Co., Ltd. (Guangzhou, China).

A typical procedure for preparing the 0.5%Ni-10%Cu/SiO₂-CA(H₂) catalyst was conducted as follows: 0.426 mmol Ni(NO₃)₂·6H₂O, 7.868 mmol Cu(NO₃)₂·3H₂O, and 8.324 mmol CA (mole ratio of CA/metal = 1:1) were dissolved in 50 mL deionized water. Subsequently, 83.217 mmol TEOS was added with magnetic stirring, followed by 6 h of stirring at 60 °C to form a gel. The gel was dried at 120 °C for 12 h, ground, and sieved (100 mesh) to yield the 0.5%Ni-10%Cu/SiO₂-CA precursor. Reduction in 99.999% H₂ at 400 °C for 2 h produced the 0.5%Ni-10%Cu/SiO₂-CA(H₂) catalyst. The 1%Ni-10%Cu/SiO₂-CA was prepared similarly, using 0.852 mmol Ni(NO₃)₂·6H₂O and 8.72 mmol CA, while maintaining constant amounts of Cu(NO₃)₂·3H₂O and TEOS.

3.2. Reaction Process

The furfural hydrogenation was performed in a 30 mL PID-controlled stainless steel reactor with magnetic stirring (1000 rpm). Each reaction used 0.32 g furfuryl, 0.089 g catalyst, and 2.88 g isopropanol. The reaction was conducted at 55 °C and 2 MPa. After cooling to room temperature, the reaction mixture was filtered, and the filtrate was analyzed by a Shimadzu (Kyoto, Japan) GC-2010 Pro gas chromatograph (GC) equipped with a flame ionization detector (FID) and an HP-INNOW AX column (Agilent 19091 N-1311, Santa Clara, CA, USA, 30 m × 0.25 mm × 0.25 μm). The injector, column, and FID temperatures were fixed at 250 °C, 80 °C, and 280 °C, respectively. The furfural and furfuryl alcohol concentrations were determined using the internal standard method.

Furfural conversion (X), product yield (Y), and product selectivity (S) were calculated as follows:

$$X = \frac{n_{\text{ninitial}} - n_{\text{final}}}{n_{\text{ninitial}}} * 100\% \tag{1}$$

$$Y = \frac{n_{\text{product}}}{n_{\text{ninitial}}} * 100\% \tag{2}$$

$$S = \frac{n_{\text{product}}}{n_{\text{ninitial}} - n_{\text{final}}} * 100\% \tag{3}$$

In Equations (1)–(3), n_{nitial} represents the initial moles of furfural, n_{final} represents the moles of residual furfural after reaction, and n_{product} represents the moles of each product.

3.3. Catalyst Characterization

X-ray powder diffraction (XRD) was conducted using a Japan RigakuD/MiniFlex600 diffractometer (Tokyo, Japan), utilizing a Cu Kα ray source (40 kV and 30 mA), with a diffraction angle scan range of 2θ = 10° to 80° and a scanning speed of 10°/min.

X-ray photoelectron spectroscopy (XPS) and Auger electron spectroscopy (AES) were conducted using a Thermo Scientific ESCALAB 250 Xi (Boston, MA, USA) with monochromatic Al Kα radiation (hv = 1486.6 eV). The binding energies of all the spectra were calibrated with a C 1s spectrum at 284.8 eV.

Transmission electron microscopy (TEM) images, scanning transmission electron microscopy (STEM) images, and energy-dispersive X-ray spectroscopy (EDS) elemental mapping of samples were obtained using a JEM-2100F microscope (JEOL, Tokyo, Japan) operating at 200 kV.

Hydrogen temperature-programmed reduction (H_2-TPR) was conducted using an Altamira Instruments 300 (Cumming, GA, USA), equipped with a TCD detector. Typically, 100 mg of the sample underwent pretreatment at 200 °C for 0.5 h in an argon flow of 50 mL/min. Following a period of cooling to 40 °C for stabilization, the TCD signal was monitored while heating the sample to 800 °C at a rate of 10 °C/min in a 30 mL/min H_2 flow.

Hydrogen temperature-programmed desorption (H_2-TPD) was performed using an Altamira Instruments 300. The test procedures were as follows: firstly, the samples were treated at 400 °C for 2 h under a 10% H_2/He gas flow, followed by switching the H_2 to He gas flow, then cooling to room temperature, followed by switching the He to 10% H_2/He gas flow to adsorb H_2 for 0.5 h. Subsequently, the He flow was reintroduced to clean the physically adsorbed H_2 on the catalyst surface, and the temperature increased from room temperature to 800 °C at a rate of 10 °C/min.

The Brunauer–Emmett–Teller (BET) surface area, pore volume, and average pore diameter of the catalysts were determined through the analysis of N_2 adsorption–desorption isotherms at 77.36 Kelvin using a Micromeritics ASAP 2460 analyzer (Norcross, GA, USA).

4. Conclusions

In this study, high-performance CuNi bimetallic catalysts for furfural hydrogenation were successfully developed by directly calcining dried sol–gel precursors under H_2

atmosphere. The effects of heat treatment methods (atmosphere and temperature) and reaction conditions (temperature and H_2 pressure) were investigated. The calcination of dried sol–gel precursors in H_2 at 400 °C directly produces well-dispersed Ni-promoted Cu nanoparticles with an average particle size of 2.2 nm. The optimal 0.5%Ni-10%Cu/SiO$_2$-CA(H$_2$) catalyst achieves a remarkable 99.4% yield of furfuryl alcohol under mild conditions (55 °C, 2 MPa H_2 and 4 h). The introduction of a small amount of Ni into Cu-based catalysts significantly increases the Cu^+/Cu^0 ratio, improves furfural adsorption, and enhances H_2 activation. The synergistic effect between Cu and Ni enables a prominent performance in the selective hydrogenation of furfural to furfuryl alcohol. These robust CuNi bimetallic catalysts represent a promising alternative to environmentally damaging Cu-Cr industrial catalysts.

Supplementary Materials: The following supporting information can be downloaded at: https://www.mdpi.com/article/10.3390/catal14100683/s1, Figure S1: XRD patterns of x%Ni-10%Cu/SiO$_2$-CA(H$_2$) with varying Ni contents, Figure S2: SEM images of (a–c) 10%Cu/SiO$_2$-CA(H$_2$) and (d–f) 0.5%Ni-10%Cu/SiO$_2$-CA(H$_2$), Figure S3: N_2 adsorption–desorption isotherms and pore size distributions of typical samples, Figure S4: Catalytic performance of (a) 10%Cu/SiO$_2$-CA(H$_2$) and (b) 0.5%Ni-10%Cu/SiO$_2$-CA(H$_2$) at different calcination temperatures in H_2, Figure S5: TG profiles of typical samples, Figure S6: XRD patterns of x%Cu/SiO$_2$-CA(H$_2$) catalysts with varying Cu contents, Figure S7: XRD patterns of the 0.5%Ni-10%Cu/SiO$_2$-CA(H$_2$) catalyst after multiple reaction cycles, Table S1: Textural properties of the typical samples, Table S2: Comparison of the catalytic performance of typical samples versus commercial catalysts, Table S3: Chemical compositions of the catalysts, Table S4: Quantitative analysis of Cu based on the XPS results, Table S5: Catalytic performance of Ni and Cu monometallic catalysts, Table S6: Reusability of 0.5%Ni-10%Cu/SiO$_2$-CA(H$_2$) catalyst.

Author Contributions: D.H.: methodology, resources, investigation, writing; Z.L.: methodology, resources, investigation; J.G.: writing, methodology; X.S.: methodology, resources; Y.L.: validation, resources, investigation, funding acquisition; S.Q.: conceptualization, validation, formal analysis, supervision, review and editing. All authors have read and agreed to the published version of the manuscript.

Data Availability Statement: The data are included in the article or Supplementary Materials.

Conflicts of Interest: The authors declare no conflicts of interest.

References

1. Tian, X.; Wang, Y.; Zeng, Z.; Dai, L.; Xu, J.; Cobb, K.; Ke, L.; Zou, R.; Liu, Y.; Ruan, R. Research progress on the role of common metal catalysts in biomass pyrolysis: A state-of-the-art review. *Green Chem.* **2022**, *24*, 3922–3942. [CrossRef]
2. Zhao, P.; Yan, J.; Shan, B.; Zhang, Y.; Zhao, Z.; Liu, L.; Su, Z.; Cheng, W.; Xu, X. Copper nanoparticles control of carbon supported copper catalysts for dimethyl carbonate synthesis: A short review. *Mol. Catal.* **2023**, *536*, 112910. [CrossRef]
3. Gong, W.; Chen, C.; Zhang, Y.; Zhou, H.; Wang, H.; Zhang, H.; Zhang, Y.; Wang, G.; Zhao, H. Efficient synthesis of furfuryl alcohol from H_2-hydrogenation/transfer hydrogenation of furfural using sulfonate group modified Cu Catalyst. *ACS Sustain. Chem. Eng.* **2017**, *5*, 2172–2180. [CrossRef]
4. Xu, X.; Dong, Y.; Hu, Q.; Si, N.; Zhang, C. Electrochemical hydrogen storage materials: State-of-the-art and future perspectives. *Energy Fuels* **2024**, *38*, 7579–7613. [CrossRef]
5. Mariscal, R.; Maireles-Torres, P.; Ojeda, M.; Sadaba, I.; Lopez Granados, M. Furfural: A renewable and versatile platform molecule for the synthesis of chemicals and fuels. *Energy Environ. Sci.* **2016**, *9*, 1144–1189. [CrossRef]
6. Li, X.; Jia, P.; Wang, T. Furfural: A promising platform compound for sustainable production of C4 and C5 chemicals. *ACS Catal.* **2016**, *6*, 7621–7640. [CrossRef]
7. Zhang, J.; Chen, J. Selective transfer hydrogenation of biomass-based furfural and 5-hydroxymethylfurfural over hydrotalcite-derived copper catalysts using methanol as a hydrogen donor. *ACS Sustain. Chem. Eng.* **2017**, *5*, 5982–5993. [CrossRef]
8. Zhou, K.; Chen, J.; Cheng, Y.; Chen, Z.; Kang, S.; Cai, Z.; Xu, Y.; Wei, J. Enhanced catalytic transfer hydrogenation of biomass-based furfural into 2-methylfuran over multifunctional Cu-Re bimetallic catalysts. *ACS Sustain. Chem. Eng.* **2020**, *8*, 16624–16636. [CrossRef]

9. Vaidyanathan, V.K.; Saikia, K.; Kumar, P.S.; Rathankumar, A.K.; Rangasamy, G.; Saratale, G.D. Advances in enzymatic conversion of biomass derived furfural and 5-hydroxymethylfurfural to value-added chemicals and solvents. *Bioresour. Technol.* **2023**, *378*, 128975. [CrossRef]
10. An, Z.; Li, J. Recent advances in the catalytic transfer hydrogenation of furfural to furfuryl alcohol over heterogeneous catalysts. *Green Chem.* **2022**, *24*, 1780–1808. [CrossRef]
11. Cao, Y.; Zhang, H.; Liu, K.; Zhang, Q.; Chen, K.-J. Biowaste-derived bimetallic Ru-MoO$_x$ catalyst for the direct hydrogenation of furfural to tetrahydrofurfuryl alcohol. *ACS Sustain. Chem. Eng.* **2019**, *7*, 12858–12866. [CrossRef]
12. Zhao, J.; Li, X.; Zhang, M.; Xu, Z.; Qin, X.; Liu, Y.; Han, L.; Li, G. Enhancing the catalytic performance of Co-N-C derived from ZIF-67 by mesoporous silica encapsulation for chemoselective hydrogenation of furfural. *Nanoscale* **2023**, *15*, 4612–4619. [CrossRef] [PubMed]
13. Zhang, J.; Li, D.-n.; Yuan, H.-r.; Wang, S.-r.; Chen, Y. Advances on the catalytic hydrogenation of biomass-derived furfural and 5-hydroxymethylfurfural. *J. Fuel Chem. Technol.* **2021**, *49*, 1752–1766. [CrossRef]
14. Chen, S.; Wojcieszak, R.; Dumeignil, F.; Marceau, E.; Royer, S. How catalysts and experimental conditions determine the selective hydroconversion of furfural and 5-hydroxymethylfurfural. *Chem. Rev.* **2018**, *118*, 11023–11117. [CrossRef]
15. Huang, S.; Yang, N.; Wang, S.; Sun, Y.; Zhu, Y. Tuning the synthesis of platinum-copper nanoparticles with a hollow core and porous shell for the selective hydrogenation of furfural to furfuryl alcohol. *Nanoscale* **2016**, *8*, 14104–14108. [CrossRef]
16. Cao, P.; Lin, L.; Qi, H.; Chen, R.; Wu, Z.; Li, N.; Zhang, T.; Luo, W. Zeolite-encapsulated Cu nanoparticles for the selective hydrogenation of furfural to furfuryl alcohol. *ACS Catal.* **2021**, *11*, 10246–10256. [CrossRef]
17. Tu, R.; Liang, K.; Sun, Y.; Wu, Y.; Lv, W.; Jia, C.Q.; Jiang, E.; Wu, Y.; Fan, X.; Zhang, B.; et al. Ultra-Dilute high-entropy alloy catalyst with core-shell structure for high-active hydrogenation of furfural to furfuryl alcohol at mild temperature. *Chem. Eng. J.* **2023**, *452*, 139526. [CrossRef]
18. Kalong, M.; Hongmanorom, P.; Ratchahat, S.; Koo-amornpattana, W.; Faungnawakij, K.; Assabumrungrat, S.; Srifa, A.; Kawi, S. Hydrogen-free hydrogenation of furfural to furfuryl alcohol and 2-methyl-furan over Ni and Co-promoted Cu/γ-Al$_2$O$_3$ catalysts. *Fuel Process. Technol.* **2021**, *214*, 106721. [CrossRef]
19. Liu, S.; Govindarajan, N.; Chan, K. Understanding activity trends in furfural hydrogenation on transition metal surfaces. *ACS Catal.* **2022**, *12*, 12902–12910. [CrossRef]
20. Jimenez-Gomez, C.P.; Cecilia, J.A.; Franco-Duro, F.I.; Pozo, M.; Moreno-Tost, R.; Maireles-Torres, P. Promotion effect of Ce or Zn oxides for improving furfuryl alcohol yield in the furfural hydrogenation using inexpensive Cu-based catalysts. *Mol. Catal.* **2018**, *455*, 121–131. [CrossRef]
21. Thongratkaew, S.; Luadthong, C.; Kiatphuengporn, S.; Khemthong, P.; Hirunsit, P.; Faungnawakij, K. Cu-Al spinel-oxide catalysts for selective hydrogenation of furfural to furfuryl alcohol. *Catal. Today* **2021**, *367*, 177–188. [CrossRef]
22. Yuan, H.; Hong, M.; Huang, X.; Qiu, W.; Dong, F.; Zhou, Y.; Chen, Y.; Gao, J.; Yang, S. Graphene chainmail shelled dilute Ni—Cu Alloy for selective and robust aqueous phase catalytic hydrogenation. *Adv. Sci.* **2024**, *11*, 2304349. [CrossRef] [PubMed]
23. Zhou, P.; Li, L.; Mosali, V.S.S.; Chen, Y.; Luan, P.; Gu, Q.; Turner, D.R.; Huang, L.; Zhang, J. Electrochemical hydrogenation of furfural in aqueous acetic acid media with enhanced 2-methylfuran selectivity using CuPd bimetallic catalysts. *Angew. Chem.-Int. Ed.* **2022**, *61*, e202117809. [CrossRef]
24. Rao, T.U.; Suchada, S.; Choi, C.; Machida, H.; Huo, Z.; Norinaga, K. Selective hydrogenation of furfural to tetrahydrofurfuryl alcohol in 2-butanol over an equimolar Ni-Cu-Al catalyst prepared by the co-precipitation method. *Energy Convers. Manag.* **2022**, *265*, 115736. [CrossRef]
25. Yu, C.; Fu, J.; Muzzio, M.; Shen, T.; Su, D.; Zhu, J.; Sun, S. CuNi nanoparticles assembled on graphene for catalytic methanolysis of ammonia borane and hydrogenation of nitro/nitrile compounds. *Chem. Mater.* **2017**, *29*, 1413–1418. [CrossRef]
26. Fu, Y.; Wang, S.; Wang, Y.; Wei, P.; Shao, J.; Liu, T.; Wang, G.; Bao, X. Enhancing electrochemical nitrate reduction to ammonia over Cu nanosheets via facet tandem catalysis. *Angew. Chem.-Int. Ed.* **2023**, *62*, e202303327. [CrossRef] [PubMed]
27. Yen, H.; Seo, Y.; Kaliaguine, S.; Kleitz, F. Role of metal-support interactions, particle size, and metal-metal synergy in CuNi nanocatalysts for H$_2$ generation. *ACS Catal.* **2015**, *5*, 5505–5511. [CrossRef]
28. Weerachawanasak, P.; Krawmanee, P.; Inkamhaeng, W.; Aires, F.J.C.S.; Sooknoi, T.; Panpranot, J. Development of bimetallic Ni-Cu/SiO$_2$ catalysts for liquid phase selective hydrogenation of furfural to furfuryl alcohol. *Catal. Commun.* **2021**, *149*, 106221. [CrossRef]
29. Zhang, J.; Jia, Z.; Yu, S.; Liu, S.; Li, L.; Xie, C.; Wu, Q.; Zhang, Y.; Yu, H.; Liu, Y.; et al. Regulating the Cu^0-Cu$^+$ ratio to enhance metal-support interaction for selective hydrogenation of furfural under mild conditions. *Chem. Eng. J.* **2023**, *468*, 143755. [CrossRef]
30. Fang, W.; Liu, S.; Steffensen, A.K.; Schill, L.; Kastlunger, G.; Riisager, A. On the role of Cu$^+$ and CuNi alloy phases in mesoporous CuNi catalyst for furfural hydrogenation. *ACS Catal.* **2023**, *13*, 8437–8444. [CrossRef]
31. Du, J.; Zhang, J.; Sun, Y.; Jia, W.; Si, Z.; Gao, H.; Tang, X.; Zeng, X.; Lei, T.; Liu, S.; et al. Catalytic transfer hydrogenation of biomass-derived furfural to furfuryl alcohol over in-situ prepared nano Cu-Pd/C catalyst using formic acid as hydrogen source. *J. Catal.* **2018**, *368*, 69–78. [CrossRef]
32. Liao, X.; Zhao, H.; Liu, R.; Luo, H.; Lv, Y.; Liu, P. Highly efficient and selective hydrogenation of furfural to furfuryl alcohol and cyclopentanone over Cu-Ni bimetallic Catalysts: The crucial role of CuNi alloys and Cu$^+$ species. *J. Catal.* **2024**, *436*, 115603. [CrossRef]

33. Zhao, H.; Liao, X.; Cui, H.; Zhu, M.; Hao, F.; Xiong, W.; Luo, H.; Lv, Y.; Liu, P. Efficient Cu-Co bimetallic catalysts for the selective hydrogenation of furfural to furfuryl alcohol. *Fuel* **2023**, *351*, 128887. [CrossRef]

34. Tang, F.; Wang, L.; Dessie Walle, M.; Mustapha, A.; Liu, Y.-N. An alloy chemistry strategy to tailoring the d-band center of Ni by Cu for efficient and selective catalytic hydrogenation of furfural. *J. Catal.* **2020**, *383*, 172–180. [CrossRef]

35. Luo, L.; Yuan, F.; Zaera, F.; Zhu, Y. Catalytic hydrogenation of furfural to furfuryl alcohol on hydrotalcite-derived $Cu_xNi_{3-x}AlO_y$ mixed-metal oxides. *J. Catal.* **2021**, *404*, 420–429. [CrossRef]

36. Islam, M.J.; Granollers Mesa, M.; Osatiashtiani, A.; Manayil, J.C.; Isaacs, M.A.; Taylor, M.J.; Tsatsos, S.; Kyriakou, G. PdCu single atom alloys supported on alumina for the selective hydrogenation of furfural. *Appl. Catal. B: Environ.* **2021**, *299*, 120652. [CrossRef]

37. Zhang, J.; Liu, Y.; Jia, Z.; Yu, S.; Liu, S.; Li, L.; Wu, Q.; Yu, H.; Liu, Y.; Jiang, X.; et al. Selective hydrogenation of furfural to furfuryl alcohol over copper-cobalt bimetallic catalyst. *Chem. Eng. J.* **2024**, *490*, 151677. [CrossRef]

38. Wang, S.; Lv, Y.; Ren, J.; Xu, Z.; Yang, Q.; Zhao, H.; Gao, D.; Chen, G. Ultrahigh selective hydrogenation of furfural enabled by modularizing hydrogen dissociation and substrate activation. *ACS Catal.* **2023**, *13*, 8720–8730. [CrossRef]

39. Wang, C.; Liu, Y.; Cui, Z.; Yu, X.; Zhang, X.; Li, Y.; Zhang, Q.; Chen, L.; Ma, L. In situ synthesis of Cu nanoparticles on carbon for highly selective hydrogenation of furfural to furfuryl alcohol by using pomelo peel as the carbon ssource. *ACS Sustain. Chem. Eng.* **2020**, *8*, 12944–12955. [CrossRef]

40. Yu, W.; Xiong, K.; Ji, N.; Porosoff, M.D.; Chen, J.G. Theoretical and experimental studies of the adsorption geometry and reaction pathways of furfural over FeNi bimetallic model surfaces and supported catalysts. *J. Catal.* **2014**, *317*, 253–262. [CrossRef]

41. Meng, X.; Wang, L.; Chen, L.; Xu, M.; Liu, N.; Zhang, J.; Yang, Y.; Wei, M. Charge-separated metal-couple-site in NiZn alloy catalysts towards furfural hydrodeoxygenation reaction. *J. Catal.* **2020**, *392*, 69–79. [CrossRef]

42. Sitthisa, S.; An, W.; Resasco, D.E. Selective conversion of furfural to methylfuran over silica-supported NiFe bimetallic catalysts. *J. Catal.* **2011**, *284*, 90–101. [CrossRef]